Eur J Nucl Med Mol Imaging (2016) 43:1304–1314
DOI 10.1007/s00259-016-3359-8

ORIGINAL ARTICLE

# Imaging characteristic of dual-phase $^{18}$F-florbetapir (AV-45/Amyvid) PET for the concomitant detection of perfusion deficits and beta-amyloid deposition in Alzheimer's disease and mild cognitive impairment

**Kun-Ju Lin[1,2] · Ing-Tsung Hsiao[1,2] · Jung-Lung Hsu[3,4] · Chin-Chang Huang[5] · Kuo-Lun Huang[5] · Chia-Ju Hsieh[1,2] · Shiaw-Pyng Wey[1,2] · Tzu-Chen Yen[1,2]**

Received: 20 September 2015 / Accepted: 28 February 2016 / Published online: 22 March 2016
© Springer-Verlag Berlin Heidelberg 2016

**Abstract**
*Purpose* We investigated dual-phase $^{18}$F-florbetapir (AV-45/Amyvid) PET imaging for the concomitant detection of brain perfusion deficits and beta-amyloid deposition in patients with Alzheimer's disease (AD) and amnestic mild cognitive impairment (MCI), and in cognitively healthy controls (HCs).
*Methods* A total of 82 subjects (24 AD patients, 44 MCI patients and 14 HCs) underwent both dual-phase $^{18}$F-AV-45 PET and MRI imaging. Dual-phase dynamic PET imaging consisted of (1) five 1-min scans obtained 1 – 6 min after tracer injection (perfusion $^{18}$F-AV-45 imaging, pAV-45), and (2) ten 1-min scans obtained 50 – 60 min after tracer injection (amyloid $^{18}$F-AV-45 imaging). Amyloid-negative MCI/AD patients were excluded. Volume of interest analysis and statistical parametric mapping of pAV-45 and $^{18}$F-AV-45 images were performed to investigate the perfusion deficits and the beta-amyloid burden in the three study groups. The associations between Mini-Mental State Examination (MMSE) scores and global perfusion deficits and amyloid deposition were investigated with linear and segmental linear correlation analyses.
*Results* HCs generally had normal pAV-45 findings, whereas perfusion deficits were evident in the hippocampus, and temporal, parietal and middle frontal cortices in both MCI and AD patients. The motor-sensory cortex was relatively preserved. MMSE scores in the entire study cohort were significantly associated with the degree of perfusion impairment as assessed by pAV-45 imaging ($r = 0.5156$, $P < 0.0001$). $^{18}$F-AV-45 uptake was significantly higher in AD patients than in the two other study groups. However, the correlation between MMSE scores and $^{18}$F-AV-45 uptake in MCI patients was more of a binary phenomenon and began in MCI patients with MMSE score 23.14 when $^{18}$F-AV-45 uptake was higher and MMSE score lower than in patients with early MCI. Amyloid deposition started in the precuneus and the frontal and temporal regions in early MCI, ultimately reaching the maximum burden in advanced MCI.
*Conclusion* Our results indicate that brain perfusion deficits and beta-amyloid deposition in AD follow different trajectories that can be successfully traced using dual-phase $^{18}$F-AV-45 PET imaging.

**Keywords** Dual-phase scan · Perfusion deficits · Amyloid · $^{18}$F-Florbetapir (AV-45/Amyvid) · Alzheimer's disease · Dementia · Mild cognitive impairment

**Electronic supplementary material** The online version of this article (doi:10.1007/s00259-016-3359-8) contains supplementary material, which is available to authorized users.

✉ Kun-Ju Lin
lin4857@adm.cgmh.org.tw

1 Department of Nuclear Medicine and Molecular Imaging Center, Linkou Chang Gung Memorial Hospital and University, 5. Fu-Hsing Street, Kuei Shan Hsiang, Taoyuan, Taiwan

2 Department of Medical Imaging and Radiological Sciences and Healthy Aging Research Center, Chang Gung University, Taoyuan, Taiwan

3 Section of Dementia and Cognitive Impairment, Department of Neurology, Linkou Chang Gung Memorial Hospital, Taoyuan, Taiwan

4 Graduate Institute of Humanities in Medicine, Taipei Medical University, Taipei, Taiwan

5 Department of Neurology, Linkou Chang Gung Memorial Hospital and University, Taoyuan, Taiwan

## Introduction

According to international workgroups convened by the Alzheimer's Association and the National Institute on Aging, there are two main classes of PET biomarkers for Alzheimer's disease (AD) [1]. The first type consists of markers of brain beta-amyloid (Aβ) deposition including $^{11}$C-Pittsburgh compound-B [2], $^{18}$F-florbetapir (AV-45/Amyvid) [3], $^{18}$F-flutemetamol (Vizamyl) [4], $^{18}$F-florbetaben (Neuraceq) [5] that can specifically be measured by amyloid PET imaging. The second class consists of markers of reduced metabolism such as $^{18}$F-fluorodeoxyglucose ($^{18}$F-FDG) [6] or perfusion $^{99m}$Tc-HM-PAO [7] whose uptake in the temporoparietal cortex reflects downstream neuronal injury. In general, the progression of cognitive decline can be seen as a continuum from normal cognition through amnestic mild cognitive impairment (MCI) to full-blown AD. Notably, such a trajectory can be traced using a PET biomarker signature characterized by a plateau of Aβ accumulation in the MCI stage followed by a progressive increase in downstream neuronal injury markers from cognitively healthy individuals to patients with AD [8].

Recent advances in PET imaging have provided the opportunity to shed more light on the dynamic biomarker model of AD through concomitant examination of both Aβ accumulation and downstream neuronal injury. Using $^{18}$F-AV-45 PET and $^{18}$F-FDG PET imaging, Landau et al. [9] demonstrated that $^{18}$F-AV-45 PET-positive cognitively healthy subjects have a greater risk of subsequent cognitive decline. However, hypometabolism on $^{18}$F-FDG PET imaging seems more reliable than amyloid accumulation as a biomarker of ongoing cognitive decline in patients with more advanced disease (i.e. MCI and AD). Similarly, Wu et al. [10] demonstrated that amyloid accumulation assessed by $^{18}$F-AV-45 PET imaging increases progressively from cognitively healthy individuals through patients with early MCI to those with late MCI, without increasing further in patients with full-blown AD. Conversely, $^{18}$F-FDG uptake continues to decrease gradually from early MCI to clinically overt AD. These findings indicate that the dissociation between amyloid deposition and brain glucose hypometabolism occurs in the MCI stage. Although combined amyloid PET and $^{18}$F-FDG PET scans would be required to shed more light on this issue, this approach is limited by high cost, the need for an additional hospital visit, and increased radiation exposure [11, 12].

Due to its highly lipophilic nature, $^{18}$F-AV-45 is characterized by an elevated first-pass influx rate ($K_1$). Consequently, early images may provide valuable $K_1$-related information as discussed previously [13–15]. Accumulating evidence indicates that $K_1$ reflects regional cerebral blood flow, which in turn is closely related to glucose metabolism measured on $^{18}$F-FDG PET imaging [16–18]. Moreover, abnormalities on perfusion-like images obtained on MRI, including arterial spin labelling (ASL), in AD patients have been shown to be closely associated with glucose hypometabolism as assessed on $^{18}$F-FDG PET imaging [19, 20]. Recently we and others have also reported that findings on early amyloid tracer images (e.g. $^{18}$F-AV-45 and $^{11}$C-Pittsburgh compound B) are highly correlated with $^{18}$F-FDG PET imaging findings, and therefore can ultimately serve as markers not only of Aβ burden but also of cerebral hypoperfusion [11, 12, 21].

The current study was designed to investigate dual-phase AV-45/Amyvid PET imaging in the concomitant detection of brain perfusion deficits and Aβ deposition in patients with AD and MCI, and in cognitively healthy controls (HCs). A single PET study providing dual information about regional brain perfusion and amyloid burden would eliminate the need for an additional hospital visit, reduce scanning time, and reduce costs. Our overall goal was to evaluate the feasibility of a single scan with two distinct time frames (an initial perfusion imaging followed by amyloid $^{18}$F-AV-45 imaging) to simultaneously track both Aβ accumulation and downstream neuronal injury. We also examined the potential associations between the imaging markers and the severity of cognitive decline as measured by the Mini-Mental State Examination (MMSE) at different stages of MCI and AD.

## Materials and methods

### Study participants

All of the study participants were recruited from the Chang Gung Dementia Center (CGDC) at Linkou, Taoyuan, Taiwan. Three groups of subjects were included, i.e. 14 HCs (mean age 66.9 ± 7.4 years), 44 MCI patients (mean age 73.4 ± 10.6 years) and 24 AD patients (mean age 71.4 ± 10.5 years). The recruitment methodology and the screening procedures have been described in detail previously [3, 22]. Briefly, all subjects underwent a neurological examination, neurocognitive evaluation and routine blood analysis. Study subjects were categorized on the basis of the consensus of panels composed of neuropsychologists, neurologists and neuroradiologists including experts in nuclear medicine. The HC subjects were volunteers in apparent good health, and none of them had a history of physical or neurological illnesses. The presence of cognitive deficits in HCs was excluded based on a thorough neuropsychological examination as described previously [3].

The diagnostic criteria for MCI were based on those proposed by Petersen et al. and the revised 2004 consensus criteria [23, 24]: (1) subjective memory complaints by the patient or an informant, (2) relatively normal performance in other cognitive domains, (3) normal activities of daily living, (4) objective memory impairment on at least one neurocognitive test of memory performance, and (5) no dementia according to DSM-IV criteria [25]. No rigid cut-off score was applied to determine objective memory impairment,

but MCI was generally determined when memory measures fell 1.0 – 1.5 standard deviations below the means for age-matched norms in Taiwan. Three cut-off Mini Mental Status Examination (MMSE) scores were used for different educational levels based on previous MMSE studies in Taiwan [26, 27]; i.e. less than 16 for illiterate subjects, less than 21 for grade school literate subjects, and less than 24 for junior high school and higher education literate subjects. These cut-off scores had a validated sensitivity of 100 % for dementia [27].

All of the AD patients met the National Institute for Neurological and Communicative Disorders and Stroke-Alzheimer's Disease and Related Disorder Association (NINDS-ADRDA) criteria for probable AD [28]. Based on MMSE scores, AD patients were divided into subgroups AD-1 (MMSE score >15, $n = 12$, mean age 71.9 ± 10.3 years) and AD-2 (MMSE score ≤15, $n = 12$, mean age 70.9 ± 11.1 years). MCI patients were further divided into three subgroups: MCI-1 (MMSE score >25, $n = 12$, mean age 71.5 ± 11.3 years), MCI-2 (MMSE score 21 – 25, $n = 20$, mean age 75.0 ± 9.5 years) and MCI-3 (MMSE score <21, $n = 12$, mean age 72.6 ± 12.0 years). The protocol was approved by the institutional review board of CGMH. Written informed consent was obtained for all subjects. In addition, the next of kin or guardians of the AD and MCI patients also gave their written informed consents if the patients could not comprehend the study protocol or could not sign their name clearly.

## Imaging protocol

$^{18}$F-AV-45 was synthesized at the cyclotron facility of Chang Gung Memorial Hospital as previously described with slight modifications [29]. The radiochemical purity of the $^{18}$F-AV-45 obtained was greater than 95 %, with a specific activity of >10, 000 Ci/mmol. All of the $^{18}$F-AV-45 scans were performed on a Biograph mCT PET/CT system (Siemens Medical Solutions, Malvern, PA) using a three-dimensional (3D) acquisition mode. After intravenous injection of 378 ± 17 MBq $^{18}$F-AV-45, two sets of images were acquired from a single PET scan as previously described [11]. In brief, dual-phase dynamic PET imaging consisted of (1) five 1-min scans obtained 1 – 6 min after tracer injection (perfusion AV-45 imaging, pAV-45), and (2) ten 1-min scans obtained 50 – 60 min after tracer injection (amyloid $^{18}$F-AV-45 imaging). PET images were reconstructed using a 3D OSEM algorithm (four iterations, 24 subsets, gaussian filter, 2 mm, zoom 3) with low-dose CT-based attenuation correction. Scatter and random corrections were performed using the correction methods provided by the manufacturer. The reconstructed images had a matrix size of 400 × 400 × 148 and a voxel size of 0.68 × 0.68 × 1.5 mm. T1-weighted MRI images were obtained from all participants to (1) exclude the presence of significant structural lesions, (2) obtain useful anatomical information, and (3) provide coregistration with PET images.

## Data analysis

All imaging data were processed and analysed using PMOD image analysis software, version 3.2 (PMOD Technologies Ltd, Zurich, Switzerland). The 3D visualization images were displayed using a BrainNet viewer [30]. The dynamic 1-min images from the early and late scan phases were initially corrected for motion and the pAV-45 and $^{18}$F-AV-45 images were each subsequently averaged. Both the pAV-45 and amyloid $^{18}$F-AV-45 images were coregistered with the corresponding T1-weighted MR images. Individual T1-weighted MR images were spatially normalized to the Montreal Neurological Institute (MNI) MRI template [31]. Spatial normalization parameters were then applied to the corresponding PET images to obtain normalized PET images in the MNI space. The modified automated anatomical labelling (AAL) atlas including 86 volumes of interest (VOIs) was applied to both normalized pAV-45 and amyloid $^{18}$F-AV-45 images [11, 32]. The 86 VOIs were grouped together into nine meta-VOIs [33] (i.e. frontal region, anterior cingulate, posterior cingulate, occipital region, parietal region excluding precuneus, precuneus, temporal region, hippocampus, and whole cerebellum) for analysis [22]. The whole cerebellum was used as the reference region to calculate the standardized uptake value ratio (SUVR) for both pAV-45 and amyloid $^{18}$F-AV-45 images [3, 34]. The global SUVR was calculated as the mean SUVR from eight cortical meta-VOIs. A global $^{18}$F-AV-45 SUVR cut-off value of 1.10 was used to define amyloid positivity [35]. Amyloid-negative HC (HC−) subjects were used for comparison and amyloid-negative MCI/AD subjects were excluded from all analyses.

## Voxel-wise analysis

In addition to VOI examination, a voxel-wise analysis of SUVR parametric images was performed by SPM5 (Welcome Department of Cognitive Neurology, Institute of Neurology, London, UK) implemented in MATLAB 2010b (MathWorks Inc., Natick, MA). All of the pAV-45 and amyloid $^{18}$F-AV-45 spatially-normalized SUVR images were smoothed using an isotropic gaussian kernel (8 mm full-width at half-maximum). A voxel-wise two-sample $t$ test was used to compare the distribution patterns of both pAV-45 and amyloid $^{18}$F-AV-45 images between HC− and the two disease groups (i.e. MCI and AD patients). The significance was determined at $P < 0.05$ with false discovery rate (FDR) correction and an extent cluster threshold ($k_E$) of greater than 50 voxels. Voxel-wise multiple regression analysis was also used to explore the correlations between MMSE scores and both pAV-45 and amyloid $^{18}$F-AV-45 parametric images in MCI and AD patients. A voxel-wise and uncorrected threshold of $P < 0.005$ with 50 extended voxels was applied to SPM $t$ maps for positive and negative correlation analyses. These

rather liberal statistical thresholds without correction were used for multiple comparison because the main goal was to compare correlation findings among methods, not to establish correlation patterns.

### Statistical analysis

Intergroup comparisons of clinical data and regional SUVR values from perfusion pAV-45 and amyloid $^{18}$F-AV-45 images were performed using the nonparametric Kruskal-Wallis test followed by the Dunn's post-hoc pair-wise multiple comparison procedure. Linear regression and segmental linear regression (piece-wise regression) [36] models were fitted to estimate the correlations between MMSE scores and global SUVR values from both pAV-45 and amyloid $^{18}$F-AV-45 images. All statistical calculations were performed using GraphPad Prism software, version 5.0 (GraphPad Inc., San Diego, CA). Two-tailed $P$ values <0.05 were considered statistically significant.

## Results

The general characteristics of the study participants are summarized in Table 1. HCs were younger than the MCI/AD patients, albeit not significantly. No significant intergroup differences were seen in terms of sex and education. The MCI/AD patients differed from the HCs in terms of both MMSE and clinical dementia rating (CDR) scores, the only exception being MCI-1 patients (who differed from the HCs only in terms of CDR score). Using a global $^{18}$F-AV-45 SUVR cut-off value of 1.10 [35], the amyloid PET-positive rates among the HCs and MCI-1 patients were relatively low (29 % and 50 %, respectively). The positive rates increased from MCI-2, MCI-3, AD-1 to AD-2 (80 %, 83 %, 92 % and 92 %, respectively). All amyloid-negative MCI/AD patients were excluded from the analysis.

### pAV-45 images in the study groups

Figure 1 shows surface plots (visualized in 3D) of average pAV-45 and $^{18}$F-AV-45 images obtained in HC− and amyloid-positive HC (HC+) subjects, and in MCI patients (three subgroups) and AD patients (two subgroups). pAV-45 images in HCs (Fig. 1a, b) showed a uniform perfusion pattern in the frontal, temporal and occipital cortices. In the MCI and AD patients, cortical perfusion was found to be reduced in parallel with decreasing MMSE scores (Fig. 1c–g). pAV-45 images in the MCI-1 and MCI-2 patients were similar to those observed in the HCs (Fig. 1c, d). However, slightly reduced perfusion was observed in the hippocampal region of the MCI-2 patients. Perfusion in the hippocampus, and temporal, parietal, superior frontal and middle frontal cortices of MCI-3 patients was moderately reduced (Fig. 1e). The pattern of hypoperfusion observed in the AD-1 patients was similar to that seen in the MCI-3 patients, despite being more extensive at the cortical level (Fig. 1f). Additional perfusion deficits were evident in the precuneus. In AD-2 patients, most cortical regions (i.e. hippocampus, and temporal, frontal and parietal cortices) exhibited marked perfusion deficits (Fig. 1g). However, perfusion in the occipital and motor-sensory cortices was relatively preserved.

### Amyloid $^{18}$F-AV-45 images in the study groups

As expected, average $^{18}$F-AV-45 images revealed very minor amyloid deposition in HC− subjects (Fig. 1h). Amyloid accumulation generally started from specific brain areas (i.e. precuneus, parietotemporal region, frontal region) and was found to be widespread in MCI and AD patients (Fig. 1j–n). Cortical

**Table 1** General characteristics of the study participants

| | HC | MCI-1 (MMSE score >25) | MCI-2 (MMSE score 21 – 25) | MCI-3 (MMSE score <21) | AD-1 (MMSE score >15) | AD-2 (MMSE score ≤15) | *P* value |
|---|---|---|---|---|---|---|---|
| No. of subjects | 10 | 6 | 16 | 10 | 11 | 11 | |
| Sex (M/F) | 6/4 | 3/3 | 9/7 | 5/5 | 2/9 | 4/7 | 0.3861 |
| Age (years) | 66.2 ± 7.5 | 71.5 ± 12.2 | 74.6 ± 9.3 | 72.8 ± 10.7 | 70.7 ± 9.9 | 70.1 ± 11.3 | 0.4551 |
| Education (years) | 13.1 ± 5.3 | 12.0 ± 5.1 | 10.4 ± 4.1 | 7.6 ± 3.1 | 9.0 ± 4.9 | 9.6 ± 3.7 | 0.0896 |
| MMSE score | 29.1 ± 0.9 | 27.5 ± 1.4 | 23.2 ± 1.6 | 16.7 ± 3.7 | 19.1 ± 1.7 | 12.2 ± 2.0 | <0.001 |
| CDR score | 0.0 ± 0.0 | 0.5 ± 0.0[a] | 0.5 ± 0.1[a] | 0.6 ± 0.2[a] | 0.6 ± 0.2[a] | 1.0 ± 0.4[b] | <0.001 |
| Duration of cognitive impairment (year) | – | 0.8 ± 0.3 | 0.9 ± 0.2 | 1.1 ± 0.2 | 1.2 ± 0.3 | 2.4 ± 0.9[c] | <0.001 |

Data are given as number or mean ± standard deviation, as appropriate

*HC* healthy controls, *MCI* mild cognitive impairment, *AD* Alzheimer's disease, *MMSE* Mini-Mental State Examination, *CDR* Clinical Dementia Rating

[a] $P < 0.001$ vs. HC

[b] $P < 0.05$ vs. MCI-1, MCI-3, AD-1; $P < 0.001$ vs. HC, MCI-2

[c] $P < 0.001$ vs. MCI-1, MCI-2, MCI-3, AD-1

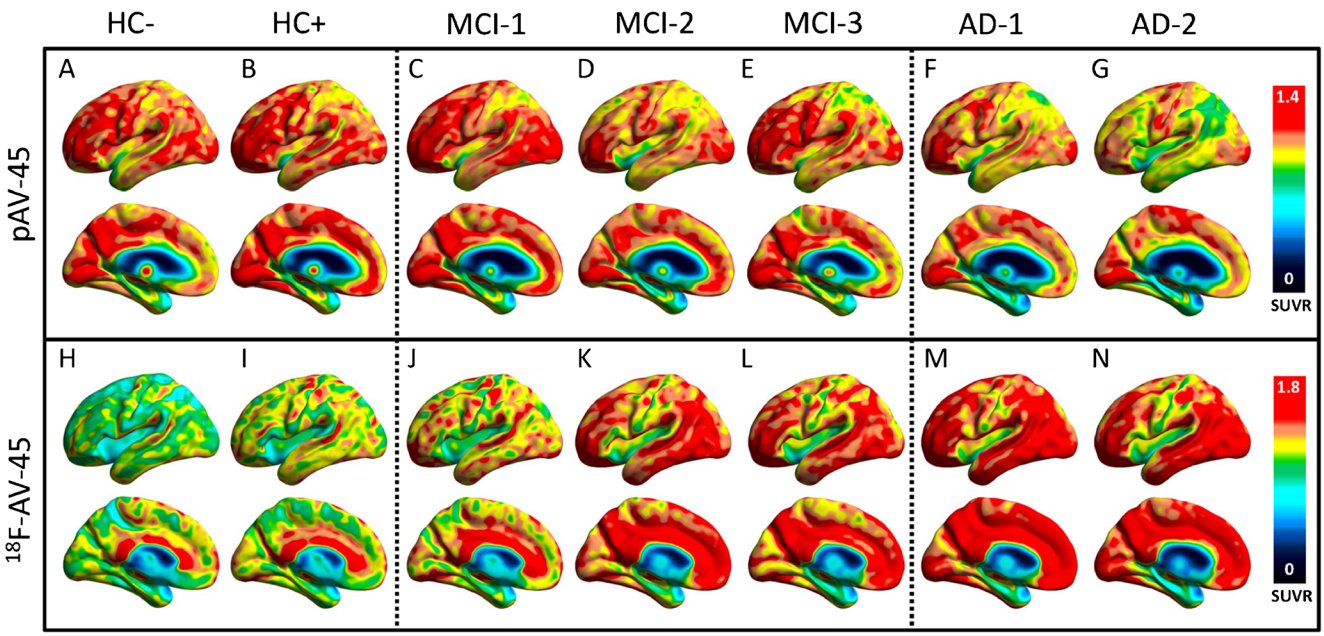


**Fig. 1** Three-dimensional visualization of average pAV-45 and amyloid $^{18}$F-AV-45 SUVR images in amyloid-negative HCs (HC-), amyloid-positive HCs (HC+), MCI patients (three subgroups), and AD patients (two subgroups)

$^{18}$F-AV-45 uptake was found to be increased in parallel with decreasing MMSE scores in MCI patients (Fig. 1j–l). The pattern of amyloid deposition in the MCI-1 patients was similar to that in HC+ subjects, despite lower accumulation in the posterior cingulate region (Fig. 1j). Increased $^{18}$F-AV-45 uptake was observed in several regions (precuneus, and frontal and temporal cortices) starting from the MCI-2 patients. In general, widespread amyloid accumulation reached a plateau in AD patients.

### Global and regional SUVR differences in the study groups

Figure 2 shows the global SUVR values from pAV-45 and amyloid $^{18}$F-AV-45 images in the study groups. Regional SUVR values are listed in the Supplementary material. The global SUVR index derived from pAV-45 images did not differ significantly between HC− subjects and MCI patients. However, significant differences were observed between HC − subjects and both AD-1 and AD-2 patients ($P<0.05$). In terms of specific regions, significant differences in perfusion were observed between HC− patients and both AD patient groups in the hippocampus. Significant hypoperfusion was also observed in the frontal and temporal cortices in AD-2 patients compared with HC subjects. A trend for reduced SUVR in the parietal cortex and precuneus was seen in the following order: HC−, MCI, AD. However, occipital SUVR was relatively preserved among the different patient groups.

The global SUVR index derived from amyloid $^{18}$F-AV-45 images was differed significantly between HC− subjects and all patient groups beyond MCI-2. Regional amyloid accumulation was significantly different between HC− subjects and all patient groups beyond MCI-2 in the frontal, temporal and occipital cortices, the anterior cingulate, and the precuneus. However, there were no significant differences between MCI and AD patients.

### Voxel-wise analysis of pAV-45 and amyloid $^{18}$F-AV-45 images

Figure 3 shows the results of parametric mapping analysis for distinguishing the different patient groups from the HC− subjects. In general, the pAV-45 perfusion deficits in the cortical regions were not significantly different between HC− subjects and MCI-1 patients (Fig. 3a, b). The extent of pAV-45 perfusion deficits significantly increased from scattered small regions to broader areas starting from late MCI to AD with declining MMSE scores (Fig. 3c–e; Supplementary Table 2). In the MCI-3 patients, significant pAV-45 SUVR reductions were observed in several small cortical regions within the frontal, superior temporal and inferior parietal cortices (Fig. 3c). Greater perfusion deficits were evident in the AD-1 patients in the precuneus, inferior parietal cortex, hippocampus and insula (Fig. 3d). Marked hypoperfusion was observed in the precuneus, and frontal and parietotemporal cortices, with relatively spared occipital and motor-sensory cortices in the AD-2 patients (Fig. 3e). Concerning Aβ deposition (Fig. 3f–j; Supplementary Table 3), significantly increased $^{18}$F-AV-45 uptake was observed in different medium-sized regions in the precuneus as well as in the middle frontal, superior frontal, middle temporal, superior temporal and inferior occipital cortices of the MCI-1 patients (Fig. 3f). Otherwise, MCI-2 to AD-2 patients displayed widespread amyloid accumulation throughout the entire brain, indicative of possible saturation (Fig. 3g–j).

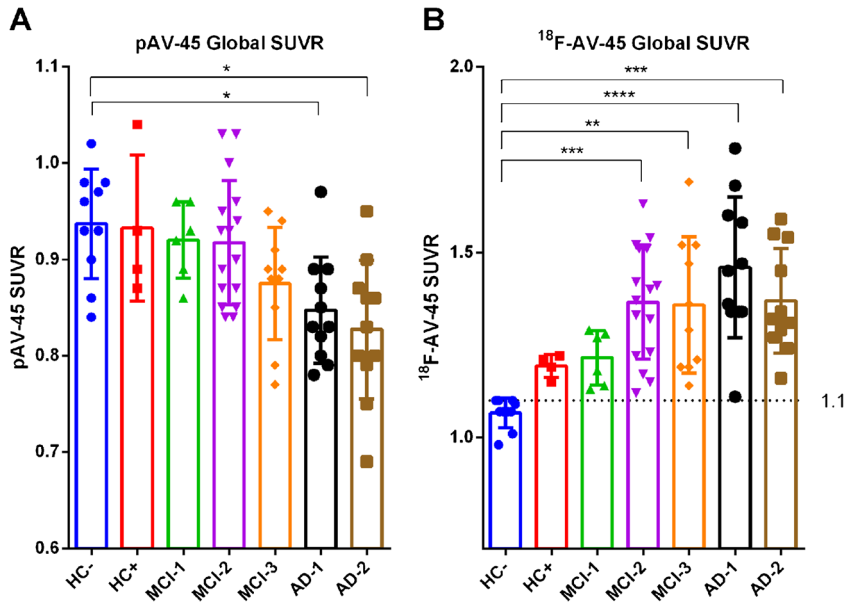


**Fig. 2** pAV-45 (**a**) and $^{18}$F-AV-45 (**b**) global SUVR values in amyloid-negative HC subjects (HC-), amyloid-positive HC subjects (HC+), MCI patients (three subgroups), and AD patients (two subgroups). The *dashed line* in **b** represents for cut-off value for amyloid positivity [35]. *$P<0.05$, **$P<0.01$, ***$P<0.001$, ****$P<0.0001$

## Correlations between MMSE scores and global indexes derived from pAV-45 and amyloid $^{18}$F-AV-45 images

Correlations between global/regional SUVR values from pAV-45 and amyloid $^{18}$F-AV-45 images and MMSE scores in MCI and AD patients are shown in Table 2. The global SUVR index derived from pAV-45 images was significantly associated with MMSE scores in the entire MCI group ($r=0.4554$, $P=0.0088$). With regard to specific regions in MCI patients, MMSE scores were significant correlated with SUVR values in the precuneus ($r=0.5021$, $P=0.0034$), hippocampus ($r=0.5427$, $P=0.0013$), and the frontal

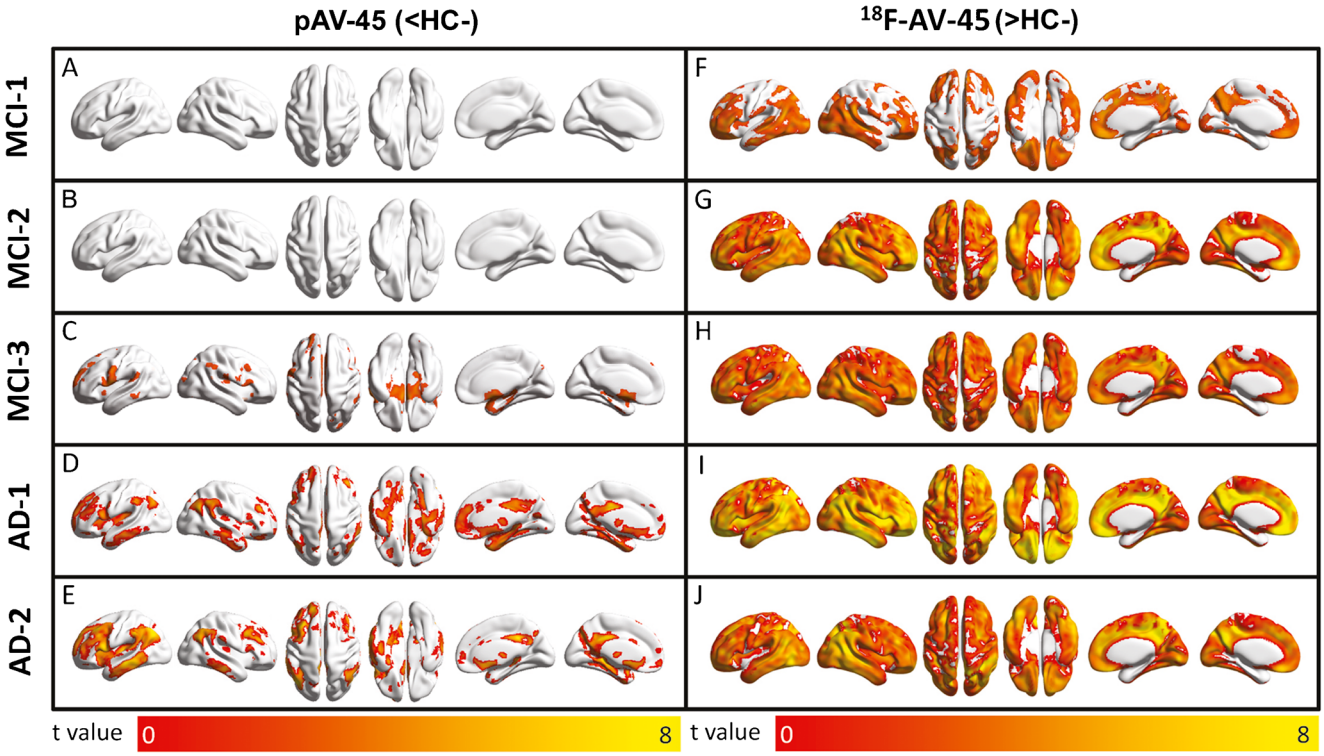


**Fig. 3** Statistical parametric maps of the hypoperfusion patterns obtained from pAV-45 images (**a**–**e**) and $^{18}$F-AV-45 images (**f**–**j**) in MCI-1 patients (**a**, **f** MMSE score >25), MCI-2 patients (**b**, **g** MMSE score 21 – 25), MCI-3 patients (**c**, **h** MMSE score <21), AD-1 patients (**d**, **i** MMSE score >15), and AD-2 patients (**e**, **j** MMSE score ≤15) compared with amyloid-negative HCs (HC−). FDR-corrected $P<0.05$ with 50 extended voxels

**Table 2** Correlations between MMSE scores and regional SUVR values obtained from dual-phase $^{18}$F-AV-45 images in the MCI and AD groups

| Region | MCI ($n=32$) | | | | AD ($n=22$) | | | |
|---|---|---|---|---|---|---|---|---|
| | pAV-45 | | $^{18}$F-AV-45 | | pAV-45 | | $^{18}$F-AV-45 | |
| | $r$ | $P$ value | $r$ | $P$ value | $r$ | $P$ value | $r$ | $P$ value |
| Frontal | 0.4357 | 0.0127 | −0.3255 | 0.0691 | 0.4147 | 0.0550 | 0.3419 | 0.1194 |
| Temporal | 0.3448 | 0.0532 | −0.1966 | 0.2808 | −0.0186 | 0.9344 | 0.2655 | 0.2324 |
| Parietal | 0.4820 | 0.0052* | −0.2058 | 0.2585 | −0.0273 | 0.9039 | 0.3892 | 0.0734 |
| Occipital | 0.2929 | 0.1038 | −0.2620 | 0.1475 | −0.0479 | 0.8325 | 0.1029 | 0.6485 |
| Anterior cingulate | 0.1192 | 0.5159 | −0.2386 | 0.1885 | 0.2081 | 0.3527 | 0.3990 | 0.0658 |
| Posterior cingulate | 0.1396 | 0.4460 | −0.2838 | 0.1154 | 0.1107 | 0.6237 | 0.4196 | 0.0519 |
| Precuneus | 0.5021 | 0.0034* | −0.3467 | 0.0519 | −0.0203 | 0.9287 | 0.2875 | 0.1944 |
| Hippocampus | 0.5427 | 0.0013* | 0.3192 | 0.0749 | 0.0259 | 0.9090 | 0.3337 | 0.1291 |
| Global index | 0.4554 | 0.0088* | −0.2424 | 0.1813 | 0.1129 | 0.6170 | 0.3723 | 0.0879 |

*MCI* mild cognitive impairment, *AD* Alzheimer's disease

*$P<0.05$

($r=0.4357$, $P=0.0127$) and parietal ($r=0.4820$, $r=0.0052$) cortices. No similar associations were identified in AD patients.The global/regional SUVR index from amyloid $^{18}$F-AV-45 images was not significantly associated with MMSE scores in either MCI or AD patients.

### Linear and segmental linear regression analyses

Linear and segmental linear regression models were fitted to identify the relationships between MMSE scores and global SUVR values from pAV-45 and amyloid $^{18}$F-AV-45 images in HC+ subjects, and MCI and AD patients (Fig. 4). Linear regression showed a significant positive correlation between MMSE scores and global SUVR values derived from pAV-45 images ($r=0.5156$, $P<0.0001$). Segmental linear regression also showed a significant negative correlation between MMSE scores and global SUVR values derived from amyloid $^{18}$F-AV-45 images ($r=0.4394$, $P=0.0178$). The MMSE score of the turning point in the segmental linear regression line was 23.14 (MCI-2 group). Figure 5 shows the 3D visualization (obtained from voxel-wise linear regression in MCI and AD patients) of the correlation coefficients between MMSE scores for both pAV-45 and amyloid $^{18}$F-AV-45 images. Significant positive correlations between MMSE scores and SUVR values from pAV-45 images were evident in both MCI and AD patients in the precuneus, hippocampus, and frontal, superior temporal and inferior parietal cortices (Fig. 5a, b; Supplementary Table 4). Compared with AD patients, correlations were generally greater and comprised larger regions in MCI subjects. There were significant negative

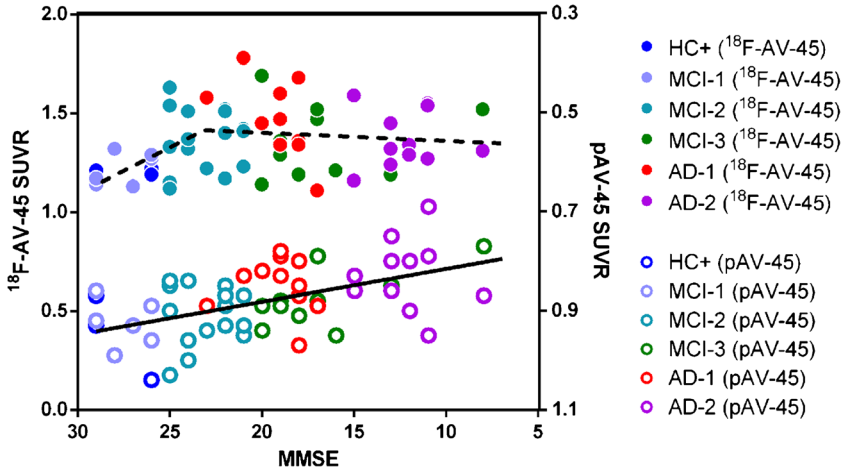


**Fig. 4** Correlations between global SUVR values from $^{18}$F-AV-45 and pAV-45 images and MMSE scores in amyloid-positive HC (HC+), MCI and AD subjects. MMSE scores showed a significant linear positive association with global SUVR values from pAV-45 images (*solid line*, $r=0.5156$, $P<0.0001$). Segmental linear regression analysis also identified a significant negative correlation between MMSE scores and global SUVR values from $^{18}$F-AV-45 images (*dashed line*, $r=0.4394$, $P=0.0178$)

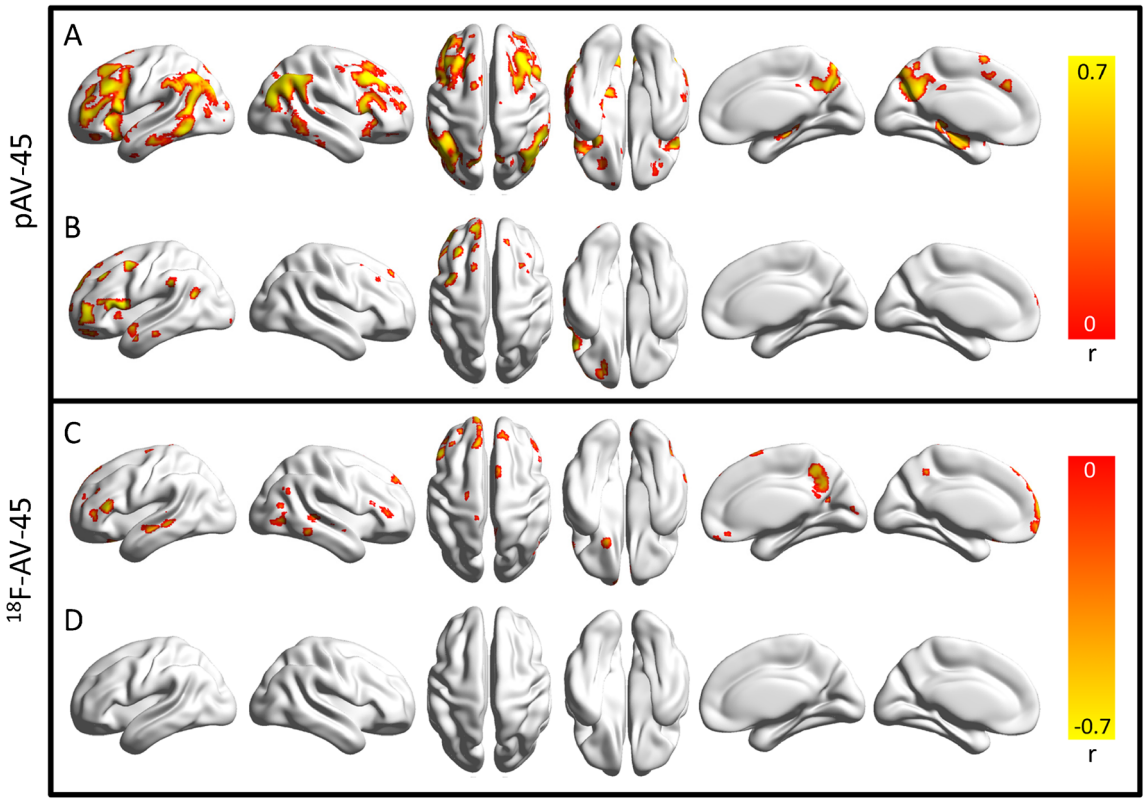


**Fig. 5** Correlation coefficient parametric maps show a positive correlation between MMSE scores and SUVR values from pAV-45 images in MCI subjects (**a** uncorrected $P<0.005$, $t>1.68$, $r>0.25$) and AD patients (**b** uncorrected $P<0.005$, $t>1.72$, $r>0.34$)., and a negative correlation between MMSE scores and SUVR values from $^{18}$F-AV-45 images only in MCI subjects (**c** uncorrected $P<0.005$, $t>1.68$, $r>0.25$), and not in AD patients (**d**)

correlations between MMSE scores and SUVR values from amyloid $^{18}$F-AV-45 images among MCI subjects only in the precuneus, anterior cingulate, and inferior occipital, inferior parietal and temporal cortices (Fig. 5c; Supplementary Table 5). No similar associations were observed in AD subjects, possibly because Aβ accumulation reached a saturation point.

## Discussion

In this study, we evaluated dual-phase pAV-45 and amyloid $^{18}$F-AV-45 imaging for the concomitant detection of brain perfusion deficits and Aβ deposition in MCI and AD patients. Regional cerebral blood flow as assessed by pAV-45 imaging is closely associated with glucose metabolism as measured by $^{18}$F-FDG PET scans [16, 21]. Conversely, $^{18}$F-AV-45 imaging is useful in the detection of brain Aβ deposition. The scanning protocol used in this study allowed the concomitant detection of both cerebral perfusion deficits and amyloid deposition in different disease stages (MCI and AD) compared with HC.

Aβ deposition was found to start from the precuneus, and frontal and temporal regions in MCI-2 patients and rapidly reached a plateau in multiple cortical areas. In contrast, perfusion deficits started from the posterior cingulate and the hippocampus in AD patients and gradually spread to other cortical regions. In line with previous findings [9], alterations in the two PET-related parameters showed a distinct imaging pattern, and Aβ deposition was observed at earlier stages of the disease than perfusion deficits. Our cross-sectional results are also in accordance with the currently accepted model of AD biomarker changes occurring at different disease stages [8].

A significant reduction in cerebral glucose metabolism has been well documented in both MCI and AD [37, 38]. Notably, brain hypometabolism has been found to be associated with the severity of cognitive decline in elderly people, and in MCI and AD patients [39–42]. Cerebral perfusion deficits assessed by ASL perfusion MRI imaging have also been linked to the risk of AD and its clinical severity [30, 43]. Interestingly, perfusion deficits on ASL MRI scans have been shown to be correlated with areas of hypometabolism on $^{18}$F-FDG PET images in AD patients [19, 44]. A previous study measuring perfusion on early $^{18}$F-AV-45 PET images has shown a highly significant correlation ($r=0.91$) with $^{18}$F-FDG PET findings [11]. Here, we expanded previous findings by showing a significant association between the results of dual-phase AV-45 PET imaging and the severity of cognitive decline in the spectrum of MCI and AD. Owing to its ability to provide

information on both perfusion and amyloid burden in a dual-phase scan, we believe that our approach may provide a more comprehensive assessment of the core pathophysiological features of AD-related neurodegeneration as compared with ASL MRI. Further studies are needed to confirm our hypothesis.

There were several limitations in our study that merit comment. First, we did not perform partial volume effect (PVE) correction for either pAV-45 or amyloid $^{18}$F-AV-45 images. As found by others, cerebral hypoperfusion may be more sensitive than brain atrophy in AD diagnosis [45]. In addition, concordance and discordance between brain perfusion and structure may be important for the differential diagnosis of dementia and staging of the disease [46]. In this work, we modified the VOI with a binary grey matter mask to minimize inclusion of both cerebrospinal fluid and white matter activity, as described in our previous work [22]. However, to improve quantification accuracy in small VOIs and to determine the possible role of brain atrophy in the reduction of perfusion, PVE correction will be included in another study. Second, some HC subjects were amyloid-positive, and some MCI and AD patients were amyloid-negative. Although these results are consistent with the range of amyloid positivity in AD and MCI patients and HC subjects observed in previous autopsy case studies [35, 47–49], we cannot exclude the possibility of imprecision of clinical evaluation. In addition, there was a relatively wide range of educational level in this population. Since we did not adjust the MMSE scores for education, the correlations between MMSE scores and perfusion deficit or amyloid burden should be interpreted with caution. A future study with a larger study group and a more uniform educational background is warranted. Last but not least, this was an exploratory imaging study from a cross-sectional analysis. The link between these dual-phase imaging markers and AD course warrants further longitudinal research.

## Conclusion

Our results indicate that brain perfusion deficits and Aβ deposition in AD follow different trajectories that can be successfully traced using dual-phase $^{18}$F-AV-45 PET scanning. HC subjects generally had normal pAV-45 findings, whereas perfusion deficits were evident in the hippocampus, and temporal, parietal and middle frontal cortices in both MCI and AD patients. The motor-sensory and occipital cortices were relatively preserved. MMSE scores in the entire study cohort were significantly associated with the degree of perfusion impairment as assessed on pAV-45 images. The uptake of $^{18}$F-AV-45 was significantly higher in AD patients than in the two other study groups. However, the correlation between MMSE scores and SUVR from $^{18}$F-AV-45 images in MCI patients was more of a binary phenomenon (i.e. segmented correlation rather than linear correlation) and began in MCI-2 patients with MMSE score 23.14 when the SUVR from $^{18}$F-AV-45 images was higher and the MMSE score lower than in MCI-1 patients. Amyloid deposition started in the precuneus and in the frontal and temporal regions in patients with early MCI, ultimately reaching the maximum burden in patients with the most advanced MCI stages. In general, brain perfusion deficits in AD are independent of Aβ accumulation.

**Acknowledgments** We thank Avid Radiopharmaceuticals Inc. (Philadelphia, PA, USA) for providing the precursor for the preparation of $^{18}$F-florbetapir.

**Compliance with ethical standards**

**Funding** This study was carried out with financial support from the National Research Program for Biopharmaceuticals, National Science Council, Taiwan (MOST 103-2314-B-182A-009, 104-2314-B-182A-083-MY2, 103-2325-B-182A-009) and grants from the Research Fund of Chang Gung Memorial Hospital (CMRPG390793).

**Conflicts of Interest** None.

**Ethical approval** All procedures performed in studies involving human participants were in accordance with the ethical standards of the institutional and/or national research committee and with the principles of the 1964 Declaration of Helsinki and its later amendments or comparable ethical standards.

**Informed consent** Informed consent was obtained from all individual participants included in the study. In addition, the next of kin or guardians of AD and MCI patients also gave their written informed consent if the patients could not comprehend the study protocol or they could not sign their name clearly.

## References

1. McKhann GM, Knopman DS, Chertkow H, Hyman BT, Jack CR, Kawas CH, et al. The diagnosis of dementia due to Alzheimer's disease: recommendations from the National Institute on Aging-Alzheimer's Association workgroups on diagnostic guidelines for Alzheimer's disease. Alzheimers Dement. 2011;7:263–9.
2. Klunk WE, Engler H, Nordberg A, Wang Y, Blomqvist G, Holt DP, et al. Imaging brain amyloid in Alzheimer's disease with Pittsburgh Compound-B. Ann Neurol. 2004;55:306–19.
3. Lin KJ, Hsu WC, Hsiao IT, Wey SP, Jin LW, Skovronsky D, et al. Whole-body biodistribution and brain PET imaging with [18F]AV-45, a novel amyloid imaging agent – a pilot study. Nucl Med Biol. 2010;37:497–508.
4. Nelissen N, Van Laere K, Thurfjell L, Owenius R, Vandenbulcke M, Koole M, et al. Phase 1 study of the Pittsburgh compound B derivative 18F-flutemetamol in healthy volunteers and patients with probable Alzheimer disease. J Nucl Med. 2009;50:1251–9.
5. Rowe CC, Ackerman U, Browne W, Mulligan R, Pike KL, O'Keefe G, et al. Imaging of amyloid beta in Alzheimer's disease with 18F-BAY94-9172, a novel PET tracer: proof of mechanism. Lancet Neurol. 2008;7:129–35.
6. Jagust WJ, Friedland RP, Budinger TF. Positron emission tomography with [18F]fluorodeoxyglucose differentiates normal pressure hydrocephalus from Alzheimer-type dementia. J Neurol Neurosurg Psychiatry. 1985;48:1091–6.

7. Smith FW, Besson JA, Gemmell HG, Sharp PF. The use of technetium-99m-HM-PAO in the assessment of patients with dementia and other neuropsychiatric conditions. J Cereb Blood Flow Metab. 1988;8:S116–22.
8. Jack CR, Knopman DS, Jagust WJ, Shaw LM, Aisen PS, Weiner MW, et al. Hypothetical model of dynamic biomarkers of the Alzheimer's pathological cascade. Lancet Neurol. 2010;9:119–28.
9. Landau SM, Mintun MA, Joshi AD, Koeppe RA, Petersen RC, Aisen PS, et al. Amyloid deposition, hypometabolism, and longitudinal cognitive decline. Ann Neurol. 2012;72:578–86.
10. Wu L, Rowley J, Mohades S, Leuzy A, Dauar MT, Shin M, et al. Dissociation between brain amyloid deposition and metabolism in early mild cognitive impairment. PLoS One. 2012;7:e47905.
11. Hsiao IT, Huang CC, Hsieh CJ, Hsu WC, Wey SP, Yen TC, et al. Correlation of early-phase 18F-florbetapir (AV-45/Amyvid) PET images to FDG images: preliminary studies. Eur J Nucl Med Mol Imaging. 2012;39:613–20.
12. Meyer PT, Hellwig S, Amtage F, Rottenburger C, Sahm U, Reuland P, et al. Dual-biomarker imaging of regional cerebral amyloid load and neuronal activity in dementia with PET and 11C-labeled Pittsburgh compound B. J Nucl Med. 2011;52:393–400.
13. Koeppe RA, Gilman S, Joshi A, Liu S, Little R, Junck L, et al. 11C-DTBZ and 18F-FDG PET measures in differentiating dementias. J Nucl Med. 2005;46:936–44.
14. Treyer V, Streffer J, Wyss MT, Bettio A, Ametamey SM, Fischer U, et al. Evaluation of the metabotropic glutamate receptor subtype 5 using PET and 11C-ABP688: assessment of methods. J Nucl Med. 2007;48:1207–15.
15. Farid K, Hong YT, Aigbirhio FI, Fryer TD, Menon DK, Warburton EA, et al. Early-phase 11C-PiB PET in amyloid angiopathy-related symptomatic cerebral hemorrhage: potential diagnostic value? PLoS One. 2015;10:e0139926.
16. Gur RC, Ragland JD, Reivich M, Greenberg JH, Alavi A, Gur RE. Regional differences in the coupling between resting cerebral blood flow and metabolism may indicate action preparedness as a default state. Cereb Cortex. 2009;19:375–82.
17. Murase K, Tanada S, Fujita H, Sakaki S, Hamamoto K. Kinetic behavior of technetium-99m-HMPAO in the human brain and quantification of cerebral blood flow using dynamic SPECT. J Nucl Med. 1992;33:135–43.
18. Wong CY, Thie J, Gaskill M, Ponto R, Hill J, Tian HY, et al. A statistical investigation of normal regional intra-subject heterogeneity of brain metabolism and perfusion by F-18 FDG and O-15 H2O PET imaging. BMC Nucl Med. 2006;6:4.
19. Chen Y, Wolk D, Reddin J, Korczykowski M, Martinez P, Musiek E, et al. Voxel-level comparison of arterial spin-labeled perfusion MRI and FDG-PET in Alzheimer disease. Neurology. 2011;77:1977–85.
20. Musiek ES, Chen Y, Korczykowski M, Saboury B, Martinez PM, Reddin JS, et al. Direct comparison of fluorodeoxyglucose positron emission tomography and arterial spin labeling magnetic resonance imaging in Alzheimer's disease. Alzheimers Dement. 2012;8:51–9.
21. Rostomian AH, Madison C, Rabinovici GD, Jagust WJ. Early [11C]PIB frames and [18F]FDG PET measures are comparable: a study validated in a cohort of AD and FTLD patients. J Nucl Med. 2011;52:173–9.
22. Huang KL, Lin KJ, Hsiao IT, Kuo HC, Hsu WC, Chuang WL, et al. Regional amyloid deposition in amnestic mild cognitive impairment and Alzheimer's disease evaluated by [18F]AV-45 positron emission tomography in Chinese population. PLoS One. 2013;8:e58974.
23. Winblad B, Palmer K, Kivipelto M, Jelic V, Fratiglioni L, Wahlund LO, et al. Mild cognitive impairment – beyond controversies, towards a consensus: report of the International Working Group on Mild Cognitive Impairment. J Intern Med. 2004;256:240–6.
24. Petersen RC, Doody R, Kurz A, Mohs RC, Morris JC, Rabins PV, et al. Current concepts in mild cognitive impairment. Arch Neurol. 2001;58:1985–92.
25. American Psychiatric Association. Diagnostic and statistical manual of mental disorders, DSM-IV. Washington, DC: American Psychiatric Association.
26. Lin RT, Lai CL, Tai CT, Liu CK, Yen YY, Howng SL. Prevalence and subtypes of dementia in southern Taiwan: impact of age, sex, education, and urbanization. J Neurol Sci. 1998;160:67–75.
27. Liu CK, Lin RT, Chen YF, Tai CT, Yen YY, Howng SL. Prevalence of dementia in an urban area in Taiwan. J Formos Med Assoc. 1996;95:762–8.
28. McKhann G, Drachman D, Folstein M, Katzman R, Price D, Stadlan EM. Clinical diagnosis of Alzheimer's disease: report of the NINCDS-ADRDA Work Group under the auspices of Department of Health and Human Services Task Force on Alzheimer's Disease. Neurology. 1984;34:939–44.
29. Yao CH, Lin KJ, Weng CC, Hsiao IT, Ting YS, Yen TC, et al. GMP-compliant automated synthesis of [(18)F]AV-45 (Florbetapir F18) for imaging beta-amyloid plaques in human brain. Appl Radiat Isot. 2010;68:2293–7.
30. Xia M, Wang J, He Y. BrainNet Viewer: a network visualization tool for human brain connectomics. PLoS One. 2013;8:e68910.
31. Mazziotta JC, Toga AW, Evans A, Fox P, Lancaster J. A probabilistic atlas of the human brain: theory and rationale for its development. The International Consortium for Brain Mapping (ICBM). Neuroimage. 1995;2:89–101.
32. Tzourio-Mazoyer N, Landeau B, Papathanassiou D, Crivello F, Etard O, Delcroix N, et al. Automated anatomical labeling of activations in SPM using a macroscopic anatomical parcellation of the MNI MRI single-subject brain. Neuroimage. 2002;15:273–89.
33. Pagani M, De Carli F, Morbelli S, Öberg J, Chincarini A, Frisoni G, et al. Volume of interest-based [18F]fluorodeoxyglucose PET discriminates MCI converting to Alzheimer's disease from healthy controls. A European Alzheimer's Disease Consortium (EADC) study. NeuroImage Clin. 2015;7:34–42.
34. Clark CM, Schneider JA, Bedell BJ, Beach TG, Bilker WB, Mintun MA, et al. Use of florbetapir-PET for imaging β-amyloid pathology. JAMA. 2011;305:275–83.
35. Johnson KA, Sperling RA, Gidicsin CM, Carmasin JS, Maye JE, Coleman RE, et al. Florbetapir (F18-AV-45) PET to assess amyloid burden in Alzheimer's disease dementia, mild cognitive impairment, and normal aging. Alzheimers Dement. 2013;9:S72–83.
36. Wagner AK, Soumerai SB, Zhang F, Ross-Degnan D. Segmented regression analysis of interrupted time series studies in medication use research. J Clin Pharm Ther. 2002;27:299–309.
37. Del Sole A, Clerici F, Chiti A, Lecchi M, Mariani C, Maggiore L, et al. Individual cerebral metabolic deficits in Alzheimer's disease and amnestic mild cognitive impairment: an FDG PET study. Eur J Nucl Med Mol Imaging. 2008;35:1357–66.
38. Silverman DH, Alavi A. PET imaging in the assessment of normal and impaired cognitive function. Radiol Clin North Am. 2005;43:67–77.
39. Habeck C, Risacher S, Lee GJ, Glymour MM, Mormino E, Mukherjee S, et al. Relationship between baseline brain metabolism measured using [18F]FDG PET and memory and executive function in prodromal and early Alzheimer's disease. Brain Imaging Behav. 2012;6:568–83.
40. Jagust W, Gitcho A, Sun F, Kuczynski B, Mungas D, Haan M. Brain imaging evidence of preclinical Alzheimer's disease in normal aging. Ann Neurol. 2006;59:673–81.
41. Landau SM, Harvey D, Madison CM, Koeppe RA, Reiman EM, Foster NL, et al. Associations between cognitive, functional, and FDG-PET measures of decline in AD and MCI. Neurobiol Aging. 2011;32:1207–18.

42. Shokouhi S, Claassen D, Kang H, Ding Z, Rogers B, Mishra A, et al. Longitudinal progression of cognitive decline correlates with changes in the spatial pattern of brain 18F-FDG PET. J Nucl Med. 2013;54:1564–9.
43. Alexopoulos P, Sorg C, Forschler A, Grimmer T, Skokou M, Wohlschlager A, et al. Perfusion abnormalities in mild cognitive impairment and mild dementia in Alzheimer's disease measured by pulsed arterial spin labeling MRI. Eur Arch Psychiatry Clin Neurosci. 2012;262:69–77.
44. Jueptner M, Weiller C. Review: does measurement of regional cerebral blood flow reflect synaptic activity? Implications for PET and fMRI. Neuroimage. 1995;2:148–56.
45. Bozzao A, Floris R, Baviera ME, Apruzzese A, Simonetti G. Diffusion and perfusion MR imaging in cases of Alzheimer's disease: correlations with cortical atrophy and lesion load. AJNR Am J Neuroradiol. 2001;22:1030–6.
46. Shimizu S, Zhang Y, Laxamana J, Miller BL, Kramer JH, Weiner MW, et al. Concordance and discordance between brain perfusion and atrophy in frontotemporal dementia. Brain Imaging Behav. 2010;4:46–54.
47. Hulette CM, Welsh-Bohmer KA, Murray MG, Saunders AM, Mash DC, McIntyre LM. Neuropathological and neuropsychological changes in "normal" aging: evidence for preclinical Alzheimer disease in cognitively normal individuals. J Neuropathol Exp Neurol. 1998;57:1168–74.
48. Pearl GS. Diagnosis of Alzheimer's disease in a community hospital-based brain bank program. South Med J. 1997;90:720–2.
49. Petersen RC, Parisi JE, Dickson DW, Johnson KA, Knopman DS, Boeve BF, et al. Neuropathologic features of amnestic mild cognitive impairment. Arch Neurol. 2006;63:665–72.